



C–H bond activation by nanosized scandium oxide clusters in gas-phase

Xiao-Nan Wu^{a,b}, Bo Xu^{a,b}, Jing-Heng Meng^{a,b}, Sheng-Gui He^{a,*}

^a Beijing National Laboratory for Molecular Sciences, State Key Laboratory for Structural Chemistry of Unstable and Stable Species, Institute of Chemistry, Chinese Academy of Sciences, Beijing 100190, PR China

^b Graduate School of Chinese Academy of Sciences, Beijing 100039, PR China

ARTICLE INFO

Article history:

Received 11 October 2011

Received in revised form

19 November 2011

Accepted 19 November 2011

Available online 26 November 2011

Keywords:

C–H bond activation

Mass spectrometry

Density functional calculation

Oxygen-centred radical

Atomic cluster

Scandium oxide

ABSTRACT

Scandium oxide cluster cations are prepared by laser ablation and reacted with *n*-butane in a fast flow reactor. A reflectron time-of-flight mass spectrometer is built to detect the cluster distribution before and after the reactions. Hydrogen atom abstraction (HAA) products $(\text{Sc}_2\text{O}_3)_N\text{H}^+$ ($N = 1-22$), $(\text{Sc}_2\text{O}_3)_N\text{O}_4\text{H}^+$ ($N = 4-22$) and their deuterated compounds are observed upon the cluster interactions with *n*-C₄H₁₀ and *n*-C₄D₁₀, respectively. This indicates that C–H bond activation of *n*-butane over atomic clusters as large as Sc₄₄O₆₆⁺ and Sc₄₄O₇₀⁺ can take place in gas phase. The experimentally determined rate constants and values of kinetic isotopic effect for HAA vary significantly with the cluster sizes. Density functional theory (DFT) calculations are performed to study the structures and reactivity of small clusters $(\text{Sc}_2\text{O}_3)_{1-3}^+$. The DFT results suggest that the experimentally observed C–H bond activation by $(\text{Sc}_2\text{O}_3)_N^+$ is facilitated by oxygen-centred radicals bridgingly bonded in the clusters. The nature of unpaired spin density distributions within the clusters may be responsible for the experimentally observed size-dependent reactivity.

© 2011 Elsevier B.V. All rights reserved.

1. Introduction

Direct transformation of alkanes that are major constituents of natural gas and oil into more valuable products is a difficult problem. Activation of the strong and localized C–H bonds that are usually chemically inert at low temperature is an essential step in alkane transformation [1–4]. It is of interest and potentially useful to generate and study chemical entities that are able to activate C–H bonds efficiently at low temperatures, preferably room temperature, which may serve as a first step to solve serious problems involved with alkane transformation at high temperature that often results in low product selectivity, primary formation of thermodynamically stable by-products (such as carbon dioxide and water in the reaction with oxygen) and other related problems of economics and environments [1,5].

It has been reported that efficient C–H bond activation can take place over many atoms, ions, and atomic clusters, among which transition metal oxide (TMO) clusters [3,4,6–11] are an important type. By using mass spectrometry, the TMO cluster systems such as $(\text{V}_2\text{O}_5)_{1-5}^+$ [12,13], $\text{V}_{4-k}\text{Y}_k\text{O}_{10-k}^+$ ($k = 1-3$) [14], $\text{V}_{4-k}\text{P}_k\text{O}_{10}^+$ ($k = 1$ and 2) [15,16], $\text{V}_2\text{O}_5(\text{SiO}_2)_{1-4}^+$ and $\text{V}_2\text{O}_6(\text{SiO}_2)_{1-4}^-$ [17,18], VAIO_4^+ and $\text{V}_{4-k}\text{Al}_k\text{O}_{11-k}^-$ ($k = 1-3$) [19,20], and others [3–5] can activate C–H bonds of methane, ethane, or *n*-butane under near

room-temperature conditions. Density functional theory (DFT) studies show that each of these clusters contains one or two oxygen atoms that have unpaired spin density (UPSD) values close to $1\mu_B$ (Bohr magnetron) and such oxygen atoms are oxygen-centred radicals ($\text{O}^{\bullet-}$). The $\text{O}^{\bullet-}$ radicals over the studied TMO clusters can effectively abstract hydrogen atoms from the reacting alkane molecules. It is noticeable that C–H bond activation of alkanes by $\text{O}^{\bullet-}$ radicals over several oxide clusters of main group elements including Mg [21], Al [22], P [23], S [24], and so on [4] have been also reported recently. So far, the largest oxide clusters that are able to activate C–H bonds of alkanes are $(\text{Al}_2\text{O}_3)_5^+$ [22] and $(\text{V}_2\text{O}_5)_5^+$ [13].

To identify further large TMO clusters that are able to activate C–H bonds, a reflectron time-of-flight mass spectrometer (Re-TOF-MS) is built and this paper reports the application of this instrument to the oxide cluster cations of the first transition metal, scandium. Scandium (Sc: $[\text{Ar}]3d^14s^2$) has only one 3d electron and scandium oxide clusters can serve as a very simple system to understand transitional metal chemistry. In addition, bulk scandium oxides are used as catalytic promoters or supports in selective reduction of nitric oxide with methane [25] and in dehydration of 1,3-diols and 1-4-diols to produce unsaturated alcohols [26,27]. Study of scandium oxide clusters may also provide molecular level insights into the related heterogeneous catalytic systems.

Matrix isolation infrared spectroscopy, photoelectron spectroscopy, and mass spectrometry have been employed to study the electronic structure and reactivity of scandium oxide species

* Corresponding author. Tel.: +86 10 62536990; fax: +86 10 62559373.

E-mail address: shengguihe@iccas.ac.cn (S.-G. He).

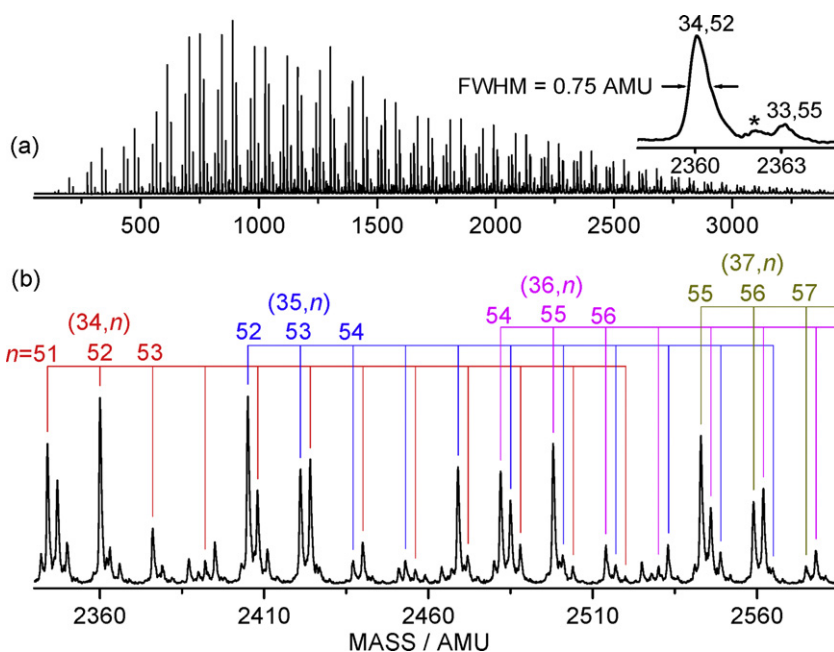


Fig. 1. An overview of a time-of-flight mass spectrum for distribution of scandium oxide cluster cations (a) and a portion of the spectrum with assignments of the peaks (b). The Sc_mO_n^+ cluster is labeled as m,n . The inset in panel (a) shows the full width at half maximum (FWHM) for the peak of $\text{Sc}_{34}^{16}\text{O}_{52}^+$ cluster. The weak peak labeled with an asterisk is due to $\text{Sc}_{34}^{16}\text{O}_{51}^{18}\text{O}^+$.

($\text{ScO}_n^{0,\pm 1}$) [28–33] while the investigations of larger ones Sc_mO_n^q ($m > 1$) are very limited [34,35] and most of which are theoretical studies [36–38]. We have recently identified that Sc_3O_6^- anion is a bi-radical with two $\text{O}^{\bullet-}$ centres and can activate two *n*-butane molecules consecutively with rate constants on the order of $10^{-10} \text{ cm}^3 \text{ molecule}^{-1} \text{ s}^{-1}$ under thermal collision conditions [35]. This study provides evidence of C–H bond activation by nanosized scandium oxide cluster cations in gas-phase.

2. Experimental and theoretical methods

2.1. Experimental details

The laser ablation and supersonic expansion cluster source coupled with a fast flow reactor is a copy of the one used in our previous studies [39–42] while the Re-TOF-MS for cluster detection is recently constructed. A brief outline of the experiments is given below. The Sc_mO_n^+ clusters are generated by laser ablation of a rotating and translating scandium metal disk (99.9%) in the presence of 0.1–0.5% O_2 seeded in a He carrier gas with backing pressure of 6 atm. A 532 nm (second harmonic of Nd^{3+} : yttrium aluminum garnet – YAG) laser with energy of 5–8 mJ/pulse and repetition rate of 10 Hz is used. The gas is controlled by a pulsed valve (General Valve, Series 9). To prevent residual water in gas handling system to form undesirable hydroxo species [$\text{Sc}_m\text{O}_n(\text{HO})_z^q$, $z > 0$], the prepared gas mixture (O_2/He) is passed through a 10 m long copper tube coil at low temperature ($T = 77 \text{ K}$) before entering into the pulsed valve. Similar treatment ($T = 273 \text{ K}$) is also applied in the use of the reactant gases (see below). The reactant gases are pulsed into the reactor 20 mm downstream from the exit of the narrow cluster formation channel by a second pulsed valve (General Valve, Series 9). By using the method in Ref. [43], the instantaneous total gas pressure in the fast flow reactor is estimated to be around 220 Pa at $T = 300 \text{ K}$. The number of collisions that a cluster (radius = 1.0 nm) experiences with the bath gas (radius = 0.05 nm, $T = 300 \text{ K}$, $P = 220 \text{ Pa}$) in the reactor is about 180 per 1 mm of forward motion. This corresponds to a collision rate of $1.8 \times 10^8 \text{ s}^{-1}$ for an approaching velocity of 1 km/s. The intra-cluster vibrations

are likely equilibrated (cooled or heated, depending on the vibrational temperature after exiting cluster formation channel with a supersonic expansion) to close to the bath gas temperature before reacting with the diluted *n*- C_4H_{10} or *n*- C_4D_{10} molecules. It may be safe to assume than the bath gas has the temperature of the wall of reactor (300 K). Our recent experiments indicate that the cluster vibrational temperature in the reactor can be close to 300 K [17,42].

After reacting in the fast flow reactor, the reactant and product ions are skimmed (3.5 mm diameter in this study for Sc_mO_n^+ clusters) into the vacuum system of a Re-TOF-MS for mass and abundance measurements. The Re-TOF-MS is home-made and the principle of design is well documented in literature [44]. A brief description of our design is given in the Supporting Information (Fig. S1). The signals from detector of the Re-TOF-MS are recorded (without pre-amplification) with a digital oscilloscope (LeCroy WaveSurfer 42Xs-A) by averaging 1000 traces of independent mass spectra (each corresponds to one laser shot). The uncertainties of the reported relative ion signals are about 10%. The mass resolution of the Re-TOF-MS is above 3000 ($M/\Delta M$) in the mass range of 2000–3000 amu (see Fig. 1 and text below). Better mass resolution (~ 4000) can be obtained if skimmers [42] with smaller diameters (2 mm) are used.

2.2. Computational details

The DFT calculations are carried out by using the Gaussian 03 program [45]. The hybrid B3LYP functional [46–48] in combination with the TZVP basis sets [49] are used to study the structures and reaction mechanisms for Sc_2O_3^+ , Sc_4O_6^+ , and Sc_6O_9^+ cluster systems. The justification of the adopted functional and basis sets for scandium oxide and hydrocarbon systems can be found in previous works [50–52]. The cage structures of Sc_4O_6^+ and Sc_6O_9^+ have been optimized previously [50] while this study further considers many other possible structures constructed based on chemical intuition and a systematic consideration of the topological conformations [17]. The reaction mechanism calculations involve geometry optimizations of reaction intermediates and transition states (TSs). The TS optimizations are performed by employing the Berny algorithm

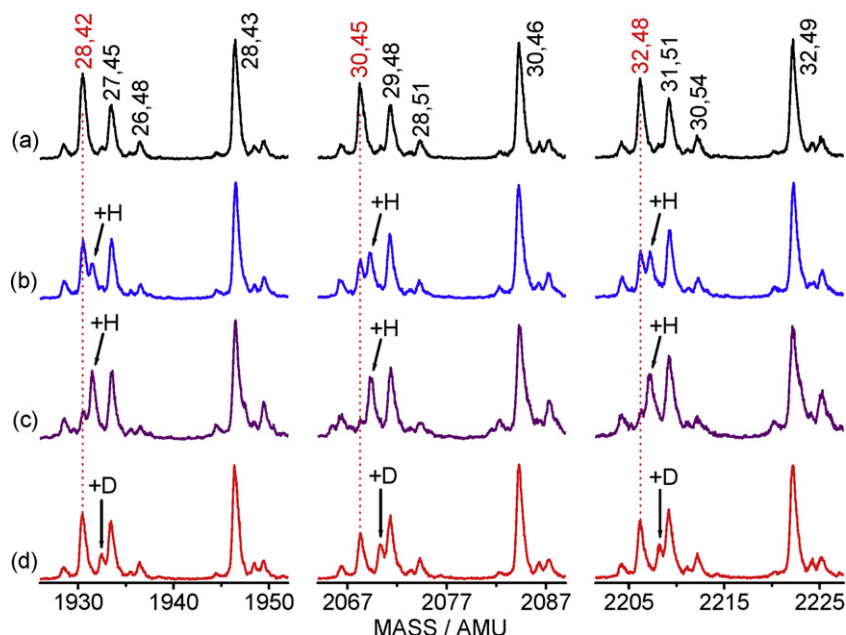


Fig. 2. Selected time-of-flight mass spectra for interactions of Sc_mO_n^+ (denoted as m,n) with He (a), 0.8 Pa $n\text{-C}_4\text{H}_{10}$ (b), 2.4 Pa $n\text{-C}_4\text{H}_{10}$ (c), and 0.8 Pa $n\text{-C}_4\text{D}_{10}$ (d) in the fast flow reactor. The product peaks $(\text{Sc}_2\text{O}_3)_{14-16}\text{H}^+$ and $(\text{Sc}_2\text{O}_3)_{14-16}\text{D}^+$ are labeled with “+H” and “+D”, respectively.

[53]. Vibrational frequency calculations are performed to check that reaction intermediates and TS species have zero and one imaginary frequency, respectively. Intrinsic reaction coordinate calculations [54,55] are also performed so that a TS connects two appropriate local minima. The DFT calculated energies reported in this study are the zero-point vibration corrected ($\Delta H_{0\text{K}}$) or the relative Gibbs free energies ($\Delta G_{298\text{K}}$) under temperature of 298.15 K and pressure of 1 atm.

3. Experimental results

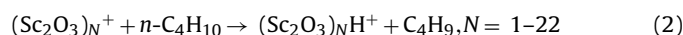
Fig. 1a plots a typical TOF mass spectrum for the distribution of Sc_mO_n^+ generated with 0.35% O_2 seeded in 6 atm He. The clusters in mass range of 50–3500 ($\text{Sc}_{1-50}\text{O}_y^+$) amu can be generated and detected as one mass spectrum. The inset spectrum in Fig. 1a indicates that for the peak of $\text{Sc}_{34}^{16}\text{O}_{52}^+$, the mass resolution is 3147 (2360.24/0.75). Note that scandium has only one stable isotope (^{45}Sc). The ^{45}Sc and ^{16}O atoms have masses of 44.9559 and 15.9949 amu, respectively. The mass of $\text{Sc}_{34}^{16}\text{O}_{52}^+$ cluster (2360.24) in unit of amu is smaller than its total mass number ($45 \times 34 + 16 \times 52 = 2362$) by about 2. A portion of the spectrum in Fig. 1a is re-plotted and labeled in Fig. 1b. The generated clusters can be classified into different scandium series such as $\text{Sc}_{34}\text{O}_n^+$ and $\text{Sc}_{35}\text{O}_n^+$. Each of the scandium series consists of several clusters with different number of oxygen atoms. For example, the number of oxygen atoms (n) in $\text{Sc}_{34}\text{O}_n^+$ series varies from 51 to 62. The leading clusters that has minimum number of oxygen atoms in Sc_m series are $(\text{Sc}_2\text{O}_3)_N^+$ for $m = 2N$ and $(\text{Sc}_2\text{O}_3)_N\text{ScO}^+$ for $m = 2N + 1$. This is very similar to the distribution of iron oxide clusters Fe_mO_n^+ in a previous study [56]. We have recently proposed that it is useful to define a value (Δ) for an oxide cluster M_mO_n^q to clarify the oxygen-richness or poorness [11,50]:

$$\Delta \equiv 2n - xm + q \quad (1)$$

in which q is the charge number and x counts the highest oxidation state of element M . The Δ value may be called *oxygen deficiency* of the cluster. The non-deficiency ($\Delta = 0$) corresponds to stoichiometric oxide clusters while positive-deficiency ($\Delta > 0$) and negative-deficiency ($\Delta < 0$) correspond to oxygen-rich and

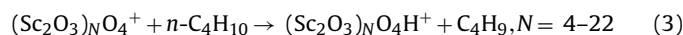
oxygen-poor clusters, respectively. The leading clusters $(\text{Sc}_2\text{O}_3)_N^+$ and $(\text{Sc}_2\text{O}_3)_N\text{ScO}^+$ are with $\Delta = 1$ and $\Delta = 0$, respectively. Fig. 1b shows that the signals of $\Delta = 0-3$ clusters ($\Delta = 1$ and 3 for Sc_{2N} series and $\Delta = 0$ and 2 for Sc_{2N+1} series) are the most intense in each scandium series. The clusters with four more oxygen atoms (+2 O_2)—that is, the oxygen-very-rich clusters with $\Delta = 8-11$ are also significantly abundant.

Fig. 2 and S2 (see Supporting Information) plot selected TOF mass spectra for the reactions of Sc_mO_n^+ with n -butane in the fast flow reactor. Fig. 2b indicates that upon the cluster interaction with 0.8 Pa $n\text{-C}_4\text{H}_{10}$ in the reactor (for about 60 μs), products that can be assigned as $\text{Sc}_{28}\text{O}_{42}\text{H}^+$, $\text{Sc}_{30}\text{O}_{45}\text{H}^+$, and $\text{Sc}_{32}\text{O}_{48}\text{H}^+$ [$(\text{Sc}_2\text{O}_3)_{14-16}\text{H}^+$] can be observed. Further increase of the $n\text{-C}_4\text{H}_{10}$ partial pressure in the reactor generates more intense signals for the above products (Fig. 2c). Meanwhile, the signal increase of $(\text{Sc}_2\text{O}_3)_{14-16}\text{H}^+$ roughly equals the signal decrease of $(\text{Sc}_2\text{O}_3)_{14-16}^+$ and the relative peak magnitudes for all of the other clusters in Fig. 2a remain unchanged within the experimental uncertainties. This indicates that each of $(\text{Sc}_2\text{O}_3)_{14-16}^+$ clusters can abstract a hydrogen atom from $n\text{-C}_4\text{H}_{10}$ to generate $(\text{Sc}_2\text{O}_3)_{14-16}\text{H}^+$ in the reactor, which is also supported by the isotopic-labeling experiment (Fig. 2d). The above reactivity pattern can be observed for all of the $\Delta = 1$ clusters $(\text{Sc}_2\text{O}_3)_N^+$ with $N = 1-22$ and the experiments thus identify the following series of reactions:



It should be pointed out that none of the $\Delta = 0$ [$(\text{Sc}_2\text{O}_3)_N\text{ScO}^+$], $\Delta = 2$ [$(\text{Sc}_2\text{O}_3)_N\text{ScO}_2^+$], and $\Delta = 3$ [$(\text{Sc}_2\text{O}_3)_N\text{O}^+$] clusters is identified to be able to abstract a hydrogen atom from n -butane although they have high abundances in the cluster source (Fig. 1).

Fig. S2 shows that the reactivity pattern of $(\text{Sc}_2\text{O}_3)_N\text{O}_4^+ / (\text{Sc}_2\text{O}_3)_N\text{O}_4\text{H}^+$ couples is very similar to that of $(\text{Sc}_2\text{O}_3)_N^+ / (\text{Sc}_2\text{O}_3)_N\text{H}^+$ in Fig. 2, suggesting the following type of reactions for $\Delta = 9$ clusters:



Note that for small systems $\text{Sc}_{1-6}\text{O}_n^+$, the abundance of the oxygen-very-rich clusters such as $(\text{Sc}_2\text{O}_3)_{1-3}\text{O}_4^+$ is very low. As a result, reaction 3 is only observed for $N > 3$.

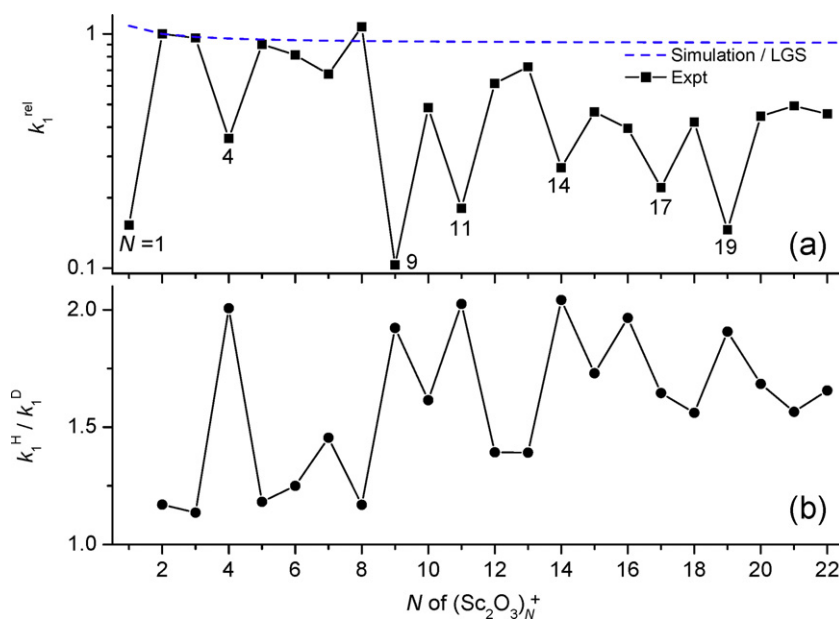


Fig. 3. Experimentally determined relative rate constants (a, k_1^{rel}) and values of kinetic isotope effect (b, $k_1^{\text{H}}/k_1^{\text{D}}$) for reactions of $(\text{Sc}_2\text{O}_3)_N^+$ with *n*-butane, in which $k_1^{\text{rel}} = k_1[(\text{Sc}_2\text{O}_3)_N^+ + n\text{-C}_4\text{H}_{10}]/k_1(\text{Sc}_4\text{O}_6^+ + n\text{-C}_4\text{H}_{10})$ and $k_1^{\text{H}}/k_1^{\text{D}} = k_1[(\text{Sc}_2\text{O}_3)_N^+ + n\text{-C}_4\text{H}_{10}]/k_1[(\text{Sc}_2\text{O}_3)_N^+ + n\text{-C}_4\text{D}_{10}]$. The experimental uncertainties for these relative rate constants are within 20% for $N=1-16$ and within 30% for $N=17-22$. A straight dashed line in panel (a) indicates the relative rate constants simulated with Langevin–Gioumousis–Stevenson (LGS) formula for ion molecule reactions [57].

The first order rate constant (k_1) in the fast flow reactor can be estimated by using the following equation:

$$k_1 = \frac{\ln(I/I_0)}{\rho \times \Delta t} \quad (4)$$

in which I and I_0 are signal magnitudes of the clusters in the presence and absence of reactant gas respectively; ρ is the molecular density of reactant gas (the method to calculate ρ has been described in Ref. [43]); and Δt is the effective reaction time in the reactor ($\sim 60 \mu\text{s}$). An absolute rate constant of $1.7 \times 10^{-10} \text{ cm}^3 \text{ molecule}^{-1} \text{ s}^{-1}$ can be determined for $k_1(\text{Sc}_4\text{O}_6^+ + n\text{-C}_4\text{H}_{10})$. This corresponds to reaction efficiency of 0.18 if the collision rate is calculated with Langevin–Gioumousis–Stevenson (LGS) formula for ion molecule reactions [57]. Because it is hard to determine accurately the ρ and Δt values in the pulse experiment, the absolute k_1 value can be systematically under or over-estimated. The systematic deviation can be within a factor of five by comparing the rate constants from our fast flow reaction experiments with those from other independent experiments for known reactions such as $\text{V}_4\text{O}_{10}^+ + \text{CH}_4 \rightarrow \text{V}_4\text{O}_{10}\text{H}^+ + \text{CH}_3$ [12,13,17].

The relative rate constants [$k_1(\text{Sc}_{2N}\text{O}_{3N}^+ + n\text{-C}_4\text{H}_{10})/k_1(\text{Sc}_4\text{O}_6^+ + n\text{-C}_4\text{H}_{10})$] that are independent of the ρ and Δt values are plotted in Fig. 3a. The values of kinetic isotope effect [KIE, defined as $k_1(\text{Sc}_{2N}\text{O}_{3N}^+ + n\text{-C}_4\text{H}_{10})/k_1(\text{Sc}_{2N}\text{O}_{3N}^+ + n\text{-C}_4\text{D}_{10})$] are shown in Fig. 3b. The relative rate constants vary significantly (by about one order of magnitude) with the size of $(\text{Sc}_2\text{O}_3)_N^+$ clusters. The relatively slow rate constants are observed for $N=1, 4, 9, 11, 14$ (see also Fig. 2), 17, and 19. The LGS formula [57] predicts that the rate constants for ion molecule reactions can vary inversely as the square root of the reduced mass. Fig. 3a indicates that this may not be used to explain the gradual decrease in the observed relative rate constants of *n*-butane with the most reactive $(\text{Sc}_2\text{O}_3)_N^+$ clusters ($N=2, 3, 5, 13, 21$). The KIE values are between about 1.1 to about 2.0 and relatively larger KIE values (Fig. 3b) generally correspond to smaller rate constants (Fig. 3a). This suggests that C–H bond activation can be the rate-limiting step in the reactions of the $(\text{Sc}_2\text{O}_3)_N^+$ clusters with *n*-butane. Since the

KIE values are not very large, it also implies that the C–H activation barrier can be small. Note that in the reaction with *n*-C₄D₁₀, the product peak $\text{Sc}_2\text{O}_3\text{D}^+$ is very weak partly due to strong scattering of Sc_2O_3^+ from the cluster beam by *n*-C₄D₁₀ that has comparable mass as this small cluster does. As a result, the KIE value in Fig. 3b is not provided for $N=1$.

4. Theoretical results

The DFT optimized structures along with the UPSD distributions for the small $\Delta=1$ clusters Sc_2O_3^+ , Sc_4O_6^+ , and Sc_6O_9^+ are shown in Fig. 4. The ground state of Sc_2O_3^+ (IS1) has three bridgingly bonded oxygen atoms (O_b) and the isomeric structure (IS2) with two O_b atoms and one terminally bonded oxygen atom (O_t) is less stable by 0.57 eV. The UPSD is delocalized over two O_b in IS1. The cage structure of Sc_4O_6^+ (IS7) still has the lowest energy, which is in agreement with the previous study [50]. Unlike Sc_2O_3^+ (IS1), in which the UPSD is delocalized, the UPSD in Sc_4O_6^+ (IS7) can be highly localized (mostly) in one O_b atom. Such O_b atoms (also in IS8) with UPSD of about $1\mu_B$ are oxygen-centred radicals and can be denoted as $\text{O}_b^{\bullet-}$. The cluster isomers (IS11, IS13–IS16) with UPSD being distributed over O_t atoms (denoted as $\text{O}_t^{\bullet-}$) are all high in energy. The $\text{O}_b^{\bullet-}$ and $\text{O}_t^{\bullet-}$ atoms in this work have essentially the same characteristics for the UPSD distributions as the free O^- anion does: UPSD of $1\mu_B$ or nearly $1\mu_B$ is distributed in one of the oxygen 2p orbitals. It is thus reasonable to include the negative signs in the superscripts of $\text{O}_b^{\bullet-}$ and $\text{O}_t^{\bullet-}$ although these oxygen atoms are in positively charged clusters. Moreover, Mulliken atomic charges on $\text{O}_b^{\bullet-}$ and $\text{O}_t^{\bullet-}$ are negative: for example, -0.59 e| on $\text{O}_b^{\bullet-}$ in IS7 and -0.47 e| on $\text{O}_t^{\bullet-}$ in IS11. It is noticeable that use of $\text{O}_b^{\bullet-}$ (or $\text{O}_t^{\bullet-}$) rather than O_b^\bullet (or O_t^\bullet) also differentiates these atomic oxygen radicals with UPSD of $1\mu_B$ from triplet O atom that has UPSD of $2\mu_B$.

The cage structures of Sc_6O_9^+ (IS22 and IS23) studied previously [50] are not the ground state. In these cages including IS7 of Sc_4O_6^+ , all of the scandium and all of the oxygen atoms are three-fold and two-fold coordinated, respectively (Sc–O spacing less than 222 pm is presume to correspond to coordination in this work). The lowest

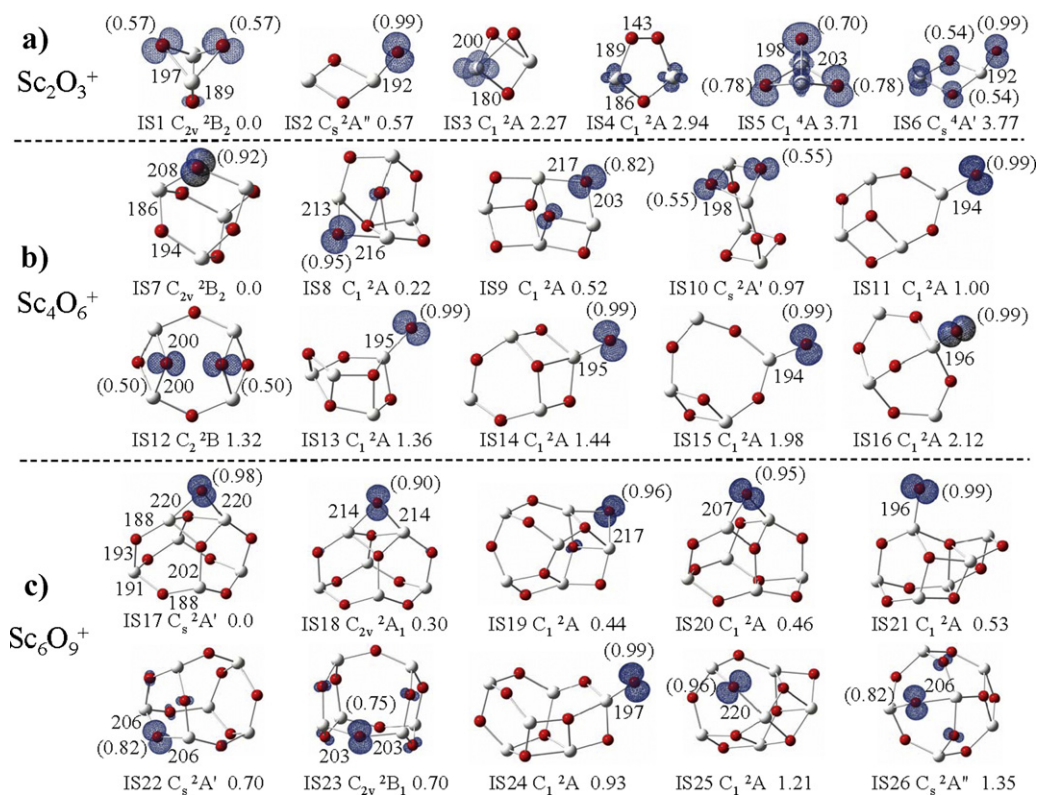
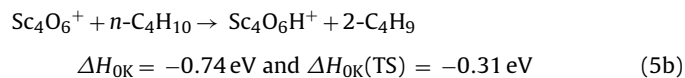
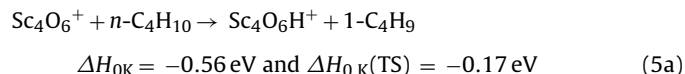


Fig. 4. Density functional theory calculated structures and profiles for unpaired spin density (UPSD) distributions of Sc_2O_3^+ (a), Sc_4O_6^+ (b), and Sc_6O_9^+ (c). The UPSD values (in the parentheses) over oxygen atoms in μ_B , some bond length in pm, and zero-point vibration corrected relative energies in eV are given.

energy structure of Sc_6O_9^+ (IS17) has two four-fold coordinated Sc atoms and two three-fold coordinated O atoms and IS17 is more stable than IS22 by 0.70 eV. The $\text{O}_b^{\bullet-}$ radicals exist in IS17–IS20 while the isomers of Sc_6O_9^+ with $\text{O}_t^{\bullet-}$ radicals (IS21 and IS24) are all significantly less stable.

Hydrogen atom abstraction (HAA) from $n\text{-C}_4\text{H}_{10}$ may result in $1\text{-C}_4\text{H}_9$ or $2\text{-C}_4\text{H}_9$ radicals. The DFT calculated energetics for $\text{Sc}_4\text{O}_6^+ (\text{IS7}) + n\text{-C}_4\text{H}_{10}$ is listed below:



in which $\Delta H_{0\text{K}}(\text{TS})$ is the energy of the transition state for C–H bond activation with respect to the separated reactants Sc_4O_6^+ and $n\text{-C}_4\text{H}_{10}$. Note that the DFT calculations can reasonably reproduce the experimental result that $2\text{-C}_4\text{H}_9$ radical is lower in energy than $1\text{-C}_4\text{H}_9$ (by 0.18 eV from DFT versus 0.13–0.15 eV from experiments [58]). As a result, the activation of the methylene group in n -butane (reaction 5b) is more exothermic as well as kinetically more favorable than that of the methyl group (reaction 5a). The DFT calculated potential energy profile for reaction 5b is shown in Fig. 5 (Fig. S3 in the Supporting Information gives a slightly less favorable reaction path). An encounter complex (IM1) with binding energy of 0.51 eV ($\Delta H_{0\text{K}}$) can be located. The C–H bond activation (IM1 \rightarrow TS \rightarrow IM2) that results in transfer of one hydrogen atom to the $\text{O}_b^{\bullet-}$ centre (see also IS7 in Fig. 4b) is subject to small barriers of 0.20/0.29 eV ($\Delta H_{0\text{K}}/\Delta G_{298\text{K}}$). The remaining part of reaction 5b (IM2 \rightarrow $\text{Sc}_4\text{O}_6\text{H}^+ + 2\text{-C}_4\text{H}_9$) is driven by highly favorable thermodynamics. Note that the $\text{O}_b^{\bullet-}$ atom in IS7 has one 2p orbital

singly occupied, which is expected to accept one hydrogen atom ($e^- + p^+$) to form closed-shell species (OH^-) that can be energetically favorable. The attack of a hydrogen atom to other O_b atoms (O_b^{2-}) without UPSD in IS7 will result in intra-cluster UPSD transfer (from $\text{O}_b^{\bullet-}$ to the reacting O_b^{2-} ion), which leads to unnecessary electronic and geometric reorganization and will be kinetically less favorable [15]. As a result, only the hydrogen atom transfer to the $\text{O}_b^{\bullet-}$ atom is given and $\text{O}_b^{\bullet-}$ can be considered as reactive centre of the cluster.

The free energy of the TS is positive (0.20 eV) with respect to the separated reactants ($\text{Sc}_4\text{O}_6^+ + n\text{-C}_4\text{H}_{10}$). As a result, one can conclude that the rate-limiting step of reaction 5b is the C–H bond activation. The small barriers in the C–H bond activation

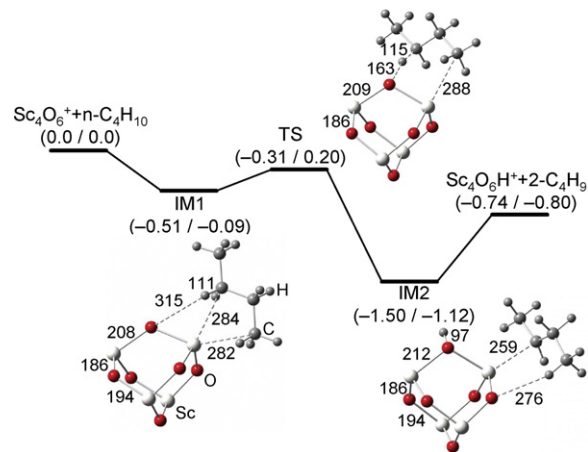


Fig. 5. Density functional theory calculated potential energy profile for $\text{Sc}_4\text{O}_6^+ (\text{IS7}, \text{C}_{2v}, ^2\text{B}_2) + n\text{-C}_4\text{H}_{10} (\text{C}_{2h}, ^1\text{A}_g) \rightarrow \text{Sc}_4\text{O}_6\text{H}^+ (\text{C}_s, ^1\text{A}') + 2\text{-C}_4\text{H}_9 (\text{C}_1, ^2\text{A})$. The relative energies $\Delta H_{0\text{K}}/\Delta G_{298\text{K}}$ in eV are given in the parentheses. Bond lengths are in pm.

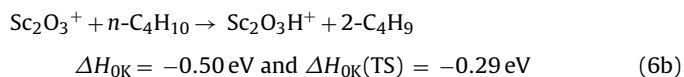
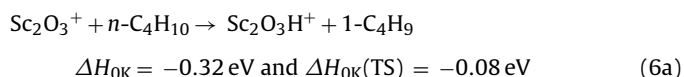
is readily surmountable by the binding energy (0.51 eV), cluster vibrational energy (0.24 eV at $T = 298$ K by DFT), and the centre-of-mass collisional energy (~ 0.25 eV) between Sc_4O_6^+ and $n\text{-C}_4\text{H}_{10}$. Note that even though the secondary C–H bond activation (reaction 5b) is more favorable than the primary C–H bond activation (reaction 5a), both channels are overall barrierless (in terms of $\Delta H_{0\text{K}}$) and exothermic and thus both probably occur experimentally. The overall barrierless energetics from the DFT is in agreement with the experimental observations of a fast reaction [$k_1(\text{Sc}_4\text{O}_6^+ + n\text{-C}_4\text{H}_{10}) = 1.7 \times 10^{-10} \text{ cm}^3 \text{ molecule}^{-1} \text{ s}^{-1}$]. The DFT determined small C–H activation barrier [$\Delta H_{0\text{K}}(\text{TS}) - \Delta H_{0\text{K}}(\text{IM1}) = 0.20$ eV in Fig. 5] is also in agreement with a KIE value [$k_1(\text{Sc}_4\text{O}_6^+ + n\text{-C}_4\text{H}_{10})/k_1(\text{Sc}_4\text{O}_6^+ + n\text{-C}_4\text{D}_{10}) = 1.2 \pm 0.1$] that is slightly larger than 1 by the experiment (Fig. 3).

5. Discussion

5.1. Size-dependent reactivity

The experimentally identified size-dependent reactivity of $(\text{Sc}_2\text{O}_3)_N^+$ shown in Fig. 3 may be rationalized with the *local spin effect* [5] that has been demonstrated for cerium oxide cluster cations [41] and anions [59] in our previous works. The UPSDs of $(\text{CeO}_2)_{2-5}^+$ clusters are delocalized, which leads to much lower reactivity of these clusters toward C–H bond activation of methane in comparison with other tetravalent metal oxide systems such as $(\text{TiO}_2)_{2-5}^+$, $(\text{ZrO}_2)_{2-4}^+$, and Hf_2O_4^+ [13] of which the UPSDs are locally distributed over a single O atom in each cluster [50]. The UPSDs in $(\text{CeO}_2)_{1-3}\text{O}^-$ cluster anions are also delocalized while in Ce_4O_9^- the UPSDs become highly localized, which is well correlated with the experimental observation of C–H bond activation of *n*-butane by the latter rather than the former clusters. The HAA by the $\text{O}^{\bullet-}$ centres with localized UPSDs of about $1\mu_{\text{B}}$ to form the OH^- species ($\text{O}^{\bullet-} + \text{H}^{\bullet} \rightarrow \text{OH}^-$) can be subject to less electronic and geometric structure reorganizations [60] involved with the reacting clusters in comparison with the HAA by the O atoms that have UPSDs of only a fraction of $1\mu_{\text{B}}$ (such O atoms can be denoted as $\text{O}^{\bullet-f}$). As a result, the HAA by $\text{O}^{\bullet-}$ can be both thermodynamically and kinetically more favorable than that by $\text{O}^{\bullet-f}$.

We thus propose that the $(\text{Sc}_2\text{O}_3)_N^+$ clusters with relatively low reactivity (Fig. 3a, $N = 1, 4, 9, 11, \dots$) have delocalized UPSDs while the clusters ($N = 2, 3, 5, 6, \dots$) with relatively high reactivity have localized UPSDs. This is true for small clusters $(\text{Sc}_2\text{O}_3)_{1-3}^+$ of which the DFT structures are available (Fig. 4). Additional DFT calculations indicate that HAA from *n*-butane by the Sc_2O_3^+ (IS1) cluster with delocalized UPSDs is less exothermic and kinetically less favorable than reaction 5:



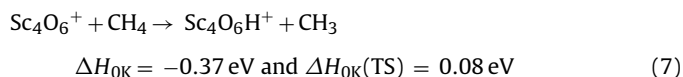
This further supports that Sc_4O_6^+ is more reactive than Sc_2O_3^+ in the reaction with *n*- C_4H_{10} . It is challenging and interesting to study larger $(\text{Sc}_2\text{O}_3)_N^+$ ($N > 3$) clusters in future with DFT calculations to verify the nature of UPSD distribution (localization and delocalization) proposed by the reactivity experiments (Fig. 3).

5.2. Bridgingly and terminally bonded oxygen-centred radicals

Most of the oxygen-centred radicals over atomic clusters identified previously [3–7,61,62] are terminally bonded ($\text{O}_t^{\bullet-}$ or $\text{O}_t^{\bullet-f}$)

while those over $(\text{Sc}_2\text{O}_3)_N^+$ ($N = 1-3$) are bridgingly bonded ($\text{O}_b^{\bullet-}$ or $\text{O}_b^{\bullet-f}$ in Fig. 4). The DFT results for large $(\text{Sc}_2\text{O}_3)_N^+$ ($N > 3$) clusters are currently unavailable. However, the similar reactivity for all of the $(\text{Sc}_2\text{O}_3)_N^+$ ($N = 1-22$) cations with *n*-butane (Fig. 3) suggests that these clusters contain oxygen-centred radicals bridgingly bonded over the clusters. This is also partly supported by the DFT results that the clusters isomers with $\text{O}_t^{\bullet-}$ are significantly less stable for small $(\text{Sc}_2\text{O}_3)_N^+$ systems (Fig. 4).

Test calculations indicate that the O–H bond energy involved with a bridging O atom can be significantly smaller than that involved with a terminal O atom. For example, the DFT calculated $\text{O}_b\text{-H}$ and $\text{O}_t\text{-H}$ bond energies of $\text{Sc}_4\text{O}_6\text{H}^+$ and $\text{V}_4\text{O}_{10}\text{H}^+$ [12,15] are 4.78 and 5.32 eV ($\Delta H_{0\text{K}}$ value), respectively. It is thus expected that the HAA by $\text{O}_b^{\bullet-}$ can be less favorable than that by $\text{O}_t^{\bullet-}$. This is supported by our previous experimental results that the $\Delta = 1$ cluster cations $(\text{TiO}_2)_{2-5}^+$, $(\text{V}_2\text{O}_5)_{1-5}^+$, and several others that contain $\text{O}_t^{\bullet-}$ radicals can abstract hydrogen atoms from methane, the most stable alkane molecules, under thermal collision conditions while no evidence of methane activation by $(\text{Sc}_2\text{O}_3)_{1-2}^+$ is observed [13]. The DFT calculations suggest that HAA from methane by Sc_4O_6^+ (IS7 in Fig. 4b) with $\text{O}_b^{\bullet-}$ is much less favorable than reaction 5 thermodynamically and kinetically:



In contrast, methane activation by $\text{O}_t^{\bullet-}$ containing cations are usually barrierless [12,19]. Note that in addition to the coordination number (two for $\text{O}_b^{\bullet-}$ and one for $\text{O}_t^{\bullet-}$) associated with the oxygen-centred radicals, other electronic effects such as number of metal valence electrons may also influence the thermodynamics and kinetics involved with C–H bond activation.

Among very few examples, $(\text{MgO})_{2-7}^+$ clusters are predicted to contain $\text{O}_b^{\bullet-}$ or $\text{O}_b^{\bullet-f}$ radicals [63]. It turns out that Mg_2O_2^+ can activate propane and butane but can not activate methane although the diatomic ion MgO^+ that has $\text{O}_t^{\bullet-}$ radical reacts with methane very efficiently to generate MgOH^+ [$k_1 = (3.9 \pm 1.3) \times 10^{-10} \text{ cm}^3 \text{ molecule}^{-1} \text{ s}^{-1}$] [21]. The reactivity of Mg_2O_2^+ and $(\text{Sc}_2\text{O}_3)_N^+$ is thus very similar. Aluminum, scandium, and iron are typical trivalent metal elements in the periodic table. The $(\text{Al}_2\text{O}_3)_4^+$ and possibly $(\text{Al}_2\text{O}_3)_{3,5}^+$ cations have $\text{O}_t^{\bullet-}$ rather than $\text{O}_b^{\bullet-}$ radicals and all of these clusters can activate methane [22]. Our test experiments indicate that $(\text{Fe}_2\text{O}_3)_{1-3}^+$ cannot activate *n*-butane [5,64]. As a result, the reactivity of $(\text{Sc}_2\text{O}_3)_N^+$ is generally in between $(\text{Al}_2\text{O}_3)_N^+$ and $(\text{Fe}_2\text{O}_3)_N^+$ in terms of C–H bond activation.

5.3. Oxygen-centred radicals over nanosized atomic clusters in gas-phase

A systematic DFT study indicates that for most of the early transition metals, the oxide clusters M_mO_n^q ($m = 1-3$) with $\Delta = 1$ all contain oxygen-centred radicals. These metals include groups 3–7 and 3d–5d elements except Cr and Mn [50]. The DFT result supports and is supported by available observations that the experimentally generated $\Delta = 1$ clusters are able to abstract hydrogen atoms from alkane molecules or deliver oxygen atoms to alkenes, alkynes, etc. under thermal collision conditions [12–24,41,59,62,65–69]. It is difficult to perform reliable DFT calculations on nanosized atomic clusters such as $(\text{Sc}_2\text{O}_3)_N^+$ ($N \geq 15$) [70]. It is also possible that each of these nanosized atomic clusters generated in gas phase may have different geometric structures. However, the experimental result that efficient C–H bond activation takes place over the $\Delta = 1$ clusters [$(\text{Sc}_2\text{O}_3)_N^+$] rather than the highly abundant $\Delta = 0$ [$(\text{Sc}_2\text{O}_3)_N\text{ScO}^+$], 2 [$(\text{Sc}_2\text{O}_3)_N\text{ScO}_2^+$], and 3 [$(\text{Sc}_2\text{O}_3)_N\text{O}^+$]

clusters (Fig. 1) quickly suggests that each of these $\Delta=1$ series contains unique reactive centres – that is, the oxygen-centred radicals, as revealed by the DFT calculations for small clusters (Fig. 4).

By studying CO oxidation, we have recently demonstrated that cerium oxide cluster series $(\text{CeO}_2)_N\text{O}^-$ can contain $\text{O}^{\bullet-}$ radicals for N up to 21 ($\text{Ce}_{21}\text{O}_{43}^-$) [59]. This study further extends the size of the $\text{O}^{\bullet-}$ containing atomic clusters up to $\text{Sc}_{44}\text{O}_{66}^+$ of which the geometrical size is about 1.36 nm [70]. It is important to point out that in this size region, *each atom still counts* because the reactivity of $\text{Sc}_{44}\text{O}_{66}^+$ in the reaction with *n*-butane is very different from that of $\text{Sc}_{44}\text{O}_{67}^+$. Note that the $\text{O}^{\bullet-}$ radicals over bulk systems can be characterized by methods such as electron spin resonance spectroscopy in condensed-phase studies [71,72]. The gas-phase cluster study is a bottom-up strategy that is able to provide mechanistic details for oxygen-centred radicals (and possibly other transient species that are hard to generate and control in condensed-phase studies) under isolated and well controlled conditions. The study of other cluster systems with current experimental setup is being carried out in order to further understand C–H bond activation by atomic oxygen radicals.

5.4. The $\Delta=9$ clusters

Most of the oxide clusters that are able to abstract hydrogen atoms from alkanes reported in literature are the least-oxygen-rich ($\Delta=1$) [11]. Only a few more oxygen-rich ($\Delta>1$) clusters, Sc_3O_6^- ($\Delta=2$) [35], Sc_3O_7^- ($\Delta=4$) [5], La_3O_7^- ($\Delta=4$) [73], Zr_2O_8^- ($\Delta=7$) [74], and Al_2O_7^+ ($\Delta=9$) [75] have been reported to be able to activate butane, ethane, or methane. A series of clusters $(\text{Sc}_2\text{O}_3)_N\text{O}_4^+$ ($N=4$ –22) with $\Delta=9$ is identified to react with *n*-butane in this work (Fig. S2 and reaction 3). It is hard to perform reliable DFT studies on large clusters such as $(\text{Sc}_2\text{O}_3)_4\text{O}_4^+$ ($=\text{Sc}_8\text{O}_{16}^+$) at present. The theoretical results on Al_2O_7^+ [$=(\text{Al}_2\text{O}_3)_4\text{O}_4^+$] [75] hint that the $(\text{Sc}_2\text{O}_3)_N\text{O}_4^+$ clusters may contain two weakly bonded O_2 units on the parent moieties of $(\text{Sc}_2\text{O}_3)_N^+$, so the oxygen-centred radicals of $(\text{Sc}_2\text{O}_3)_N^+$ are kept in $(\text{Sc}_2\text{O}_3)_N\text{O}_4^+$, which results in reaction 3. In order to have a good understanding of the $\Delta=9$ cluster series, it is also necessary to study in future why $(\text{Sc}_2\text{O}_3)_N\text{O}_4^+$ ($\Delta=9$) is more abundant than $(\text{Sc}_2\text{O}_3)_N\text{O}_2^+$ ($\Delta=5$) in the cluster distribution (Fig. 1) and why $(\text{Sc}_2\text{O}_3)_N\text{O}_2\text{H}^+$ is not produced upon the cluster interaction with *n*-butane in the reactor.

6. Conclusion

By using a reflectron time-of-flight mass spectrometer, hydrogen atom abstraction from *n*-butane is identified over two series of scandium oxide cluster cations: $(\text{Sc}_2\text{O}_3)_N^+$ ($N=1$ –22) and $(\text{Sc}_2\text{O}_3)_N\text{O}_4^+$ ($N=4$ –22). The size of atomic clusters that are able to activate alkane C–H bonds is extended to nanosizes (~ 1.36 nm for $\text{Sc}_{44}\text{O}_{66}^+$). The experimentally determined rate constants for reactions of $(\text{Sc}_2\text{O}_3)_N^+$ with *n*-butane vary within about one order magnitude and relatively slow reactions are observed at $N=1, 4, 9, 11, 14, 17,$ and 19 . Density functional theory calculations suggest that the experimentally observed C–H bond activation is facilitated by oxygen-centred radicals bridgingly bonded in $(\text{Sc}_2\text{O}_3)_N^+$. The lowest energy structure of Sc_4O_6^+ cluster is a cage while the cage structure of Sc_6O_9^+ is significantly less stable than the ground state. The $(\text{Sc}_2\text{O}_3)_{2,3}^+$ and Sc_2O_3^+ have localized and delocalized unpaired spin density distributions, respectively. This correlates with the experimentally observed relatively high reactivity of $(\text{Sc}_2\text{O}_3)_{2,3}^+$ over Sc_2O_3^+ , indicating that the local spin distribution within the clusters is responsible for the size-dependent reactivity of $(\text{Sc}_2\text{O}_3)_N^+$.

Acknowledgments

This work is supported by Chinese Academy of Sciences (Knowledge Innovation Program KJCX2-EW-H01, Hundred Talents Fund), the National Natural Science Foundation of China (No. 20933008), and Major Research Plan of China (No. 2011CB932302).

Appendix A. Supplementary data

Supplementary data associated with this article can be found, in the online version, at doi:10.1016/j.ijms.2011.11.011.

References

- [1] J.A. Labinger, J.E. Bercaw, *Nature* 417 (2002) 507–514.
- [2] D. Balcells, E. Clot, O. Eisenstein, *Chem. Rev.* 110 (2010) 749–823.
- [3] J. Roithová, D. Schröder, *Chem. Rev.* 110 (2009) 1170–1211.
- [4] H. Schwarz, *Angew. Chem. Int. Ed.* 50 (2011) 10096–10115.
- [5] X.-L. Ding, X.-N. Wu, Y.-X. Zhao, S.-G. He, *Acc. Chem. Res.* (2011), doi:10.1021/ar2001364.
- [6] A.W. Castleman Jr., *Catal. Lett.* 141 (2011) 1243–1253.
- [7] H.-J. Zhai, L.-S. Wang, *Chem. Phys. Lett.* 500 (2010) 185–195.
- [8] R.A.J. O'Hair, G.N. Khairallah, *J. Cluster Sci.* 15 (2004) 331–363.
- [9] K.R. Asmis, J. Sauer, *Mass. Spectrom. Rev.* 26 (2007) 542–562.
- [10] Y. Gong, M.-F. Zhou, L. Andrews, *Chem. Rev.* 109 (2009) 6765–6808.
- [11] Y.-X. Zhao, X.-N. Wu, J.-B. Ma, S.-G. He, X.-L. Ding, *Phys. Chem. Chem. Phys.* 13 (2011) 1925–1938.
- [12] S. Feyel, J. Döbler, D. Schröder, J. Sauer, H. Schwarz, *Angew. Chem. Int. Ed.* 45 (2006) 4681–4685.
- [13] Y.-X. Zhao, X.-N. Wu, Z.-C. Wang, S.-G. He, X.-L. Ding, *Chem. Commun.* 46 (2010) 1736–1738.
- [14] Z.-Y. Li, Y.-X. Zhao, X.-N. Wu, X.-L. Ding, S.-G. He, *Chem. Eur. J.* 17 (2011) 11728–11733.
- [15] J.-B. Ma, X.-N. Wu, X.-X. Zhao, X.-L. Ding, S.-G. He, *Phys. Chem. Chem. Phys.* 12 (2010) 12223–12228.
- [16] N. Dietl, R.F. Höckendorf, M. Schlangen, M. Lerch, M.K. Beyer, H. Schwarz, *Angew. Chem. Int. Ed.* 50 (2011) 1430–1434.
- [17] X.-L. Ding, Y.-X. Zhao, X.-N. Wu, Z.-C. Wang, J.-B. Ma, S.-G. He, *Chem. Eur. J.* 16 (2010) 11463–11470.
- [18] Y.-X. Zhao, X.-N. Wu, J.-B. Ma, S.-G. He, X.-L. Ding, *J. Phys. Chem. C* 114 (2010) 12271–12279.
- [19] Z.-C. Wang, X.-N. Wu, Y.-X. Zhao, J.-B. Ma, X.-L. Ding, S.-G. He, *Chem. Phys. Lett.* 489 (2010) 25–29.
- [20] Z.-C. Wang, X.-N. Wu, Y.-X. Zhao, J.-B. Ma, X.-L. Ding, S.-G. He, *Chem. Eur. J.* 17 (2011) 3449–3457.
- [21] D. Schröder, J. Roithová, *Angew. Chem. Int. Ed.* 45 (2006) 5705–5708.
- [22] S. Feyel, J. Döbler, R. Höckendorf, M.K. Beyer, J. Sauer, H. Schwarz, *Angew. Chem. Int. Ed.* 47 (2008) 1946–1950.
- [23] N. Dietl, M. Engeser, H. Schwarz, *Angew. Chem. Int. Ed.* 48 (2009) 4861–4863.
- [24] G. de Petris, A. Troiani, M. Rosi, G. Angelini, O. Ursini, *Chem. Eur. J.* 15 (2009) 4248–4252.
- [25] J.-Y. Ying, M.D. Fokema, *Appl. Catal. B: Environ.* 18 (1998) 71–77.
- [26] S. Sato, R. Takahashi, T. Sodesawa, A. Igarashi, H. Inoue, *Appl. Catal. A: Gen.* 328 (2007) 109–116.
- [27] S. Sato, R. Takahashi, M. Kobune, H. Inoue, Y. Izawa, H. Ohno, K. Takahashi, *Appl. Catal. A: Gen.* 356 (2009) 64–71.
- [28] M.-F. Zhou, Y. Gong, C.-F. Ding, *J. Phys. Chem. A* 111 (2007) 11572–11578.
- [29] C.W. Bauschlicher, M.-F. Zhou, L. Andrews, J.R.T. Johnson, I. Panas, A. Snis, B.O. Roos, *J. Phys. Chem. A* 103 (1999) 5463–5467.
- [30] T.D. Crawford, S.J. Kim, *J. Phys. Chem. A* 108 (2004) 3097–3102.
- [31] E.P.F. Lee, D.K.W. Mok, F.T. Chau, J.M. Dyke, *J. Comput. Chem.* 30 (2009) 337–345.
- [32] D.E. Clemmer, N. Aristov, P.B. Armentrout, *J. Phys. Chem.* 97 (1993) 544–552.
- [33] H.-B. Wu, L.-S. Wang, *J. Phys. Chem. A* 102 (1998) 9129–9135.
- [34] S.-H. Yang, M.B. Knickelbein, *Z. Phys. D: Atoms Mol. Cl.* 31 (1994) 199–203.
- [35] Y.-X. Zhao, J.-Y. Yuan, X.-L. Ding, W.-J. Zheng, S.-G. He, *Phys. Chem. Chem. Phys.* 13 (2011) 10084–10090.
- [36] J.R.T. Johnson, I. Panas, *Chem. Phys.* 248 (1999) 161–179.
- [37] J.-L. Wang, Y.-B. Wang, C.-F. Wu, X.-Y. Zhang, X.-J. Zhao, M.-L. Yang, *Phys. Chem. Chem. Phys.* 11 (2009) 5980–5985.
- [38] Y. Wang, X. Gong, J. Wang, *Phys. Chem. Chem. Phys.* 12 (2010) 2471–2477.
- [39] W.-G. Wang, Z.-C. Wang, S. Yin, S.-G. He, M.-F. Ge, *Chinese J. Chem. Phys.* 20 (2007) 412.
- [40] W. Xue, S. Yin, X.-L. Ding, S.-G. He, M.-F. Ge, *J. Phys. Chem. A* 113 (2009) 5302–5309.
- [41] X.-N. Wu, Y.-X. Zhao, W. Xue, Z.-C. Wang, S.-G. He, X.-L. Ding, *Phys. Chem. Chem. Phys.* 12 (2010) 3984–3997.
- [42] X.-N. Wu, J.-B. Ma, B. Xu, Y.-X. Zhao, X.-L. Ding, S.-G. He, *J. Phys. Chem. A* 115 (2011) 5238–5246.
- [43] W. Xue, Z.-C. Wang, S.-G. He, Y. Xie, E.R. Bernstein, *J. Am. Chem. Soc.* 130 (2008) 15879–15888.
- [44] B.A. Mamyryn, *Int. J. Mass Spectrom.* 206 (2001) 251–266.

- [45] M.J. Frisch, G.W. Trucks, H.B. Schlegel, G.E. Scuseria, M.A. Robb, J.R. Cheeseman, J.A. Montgomery, T. Vreven Jr., K.N. Kudin, J.C. Burant, J.M. Millam, S.S. Iyengar, J. Tomasi, V. Barone, B. Mennucci, M. Cossi, G. Scalmani, N. Rega, G.A. Petersson, H. Nakatsuji, M. Hada, M. Ehara, K. Toyota, R. Fukuda, J. Hasegawa, M. Ishida, T. Nakajima, Y. Honda, O. Kitao, H. Nakai, M. Klene, X. Li, J.E. Knox, H.P. Hratchian, J.B. Cross, V. Bakken, C. Adamo, J. Jaramillo, R. Gomperts, R.E. Stratmann, O. Yazyev, A.J. Austin, R. Cammi, C. Pomelli, J. Ochterski, P.Y. Ayala, K. Morokuma, G.A. Voth, P. Salvador, J.J. Dannenberg, V.G. Zakrzewski, S. Dapprich, A.D. Daniels, M.C. Strain, O. Farkas, D.K. Malick, A.D. Rabuck, K. Raghavachari, J.B. Foresman, J.V. Ortiz, Q. Cui, A.G. Baboul, S. Clifford, J. Cioslowski, B.B. Stefanov, A.L.G. Liu, P. Piskorz, I. Komaromi, R.L. Martin, D.J. Fox, T. Keith, M.A. Al-Laham, C.Y. Peng, A. Nanayakkara, M. Challacombe, P.M.W. Gill, B.G. Johnson, W. Chen, M.W. Wong, C. Gonzalez, J.A. Pople, Gaussian 03, Revision C. 02, Gaussian Inc., Wallingford, CT, 2004.
- [46] A.D. Becke, *Phys. Rev. A* 38 (1988) 3098–3100.
- [47] A.D. Becke, *J. Chem. Phys.* 98 (1993) 5648–5652.
- [48] C.T. Lee, W.T. Yang, R.G. Parr, *Phys. Rev. B* 37 (1988) 785–789.
- [49] A. Schäfer, C. Huber, R. Ahlrichs, *J. Chem. Phys.* 100 (1994) 5829–5835.
- [50] Y.-X. Zhao, X.-L. Ding, Y.-P. Ma, Z.-C. Wang, S.-G. He, *Theor. Chem. Acc.* 127 (2010) 449–465.
- [51] Y.-P. Ma, W. Xue, Z.-C. Wang, M.-F. Ge, S.-G. He, *J. Phys. Chem. A* 112 (2008) 3731–3741.
- [52] F. Dong, S. Heinbuch, Y. Xie, J.J. Rocca, E.R. Bernstein, Z.-C. Wang, K. Deng, S.-G. He, *J. Am. Chem. Soc.* 130 (2008) 1932–1943.
- [53] H.B. Schlegel, *J. Comput. Chem.* 3 (1982) 214–218.
- [54] C. Gonzalez, H.B. Schlegel, *J. Chem. Phys.* 90 (1989) 2154–2161.
- [55] C. Gonzalez, H.B. Schlegel, *J. Phys. Chem.* 94 (1990) 5523–5527.
- [56] S. Yin, W. Xue, X.-L. Ding, W.-G. Wang, S.-G. He, M.-F. Ge, *Int. J. Mass Spectrom.* 281 (2009) 72–78.
- [57] G. Gioumoussis, D.P. Stevenson, *J. Chem. Phys.* 29 (1958) 294–299.
- [58] L.A. Gribov, I.A. Novakov, A.I. Pavlyuchko, I.O. Kulago, B.S. Orlinson, *J. Struct. Chem.* 44 (2003) 961–969.
- [59] X.-N. Wu, X.-L. Ding, S.-M. Bai, B. Xu, S.-G. He, Q. Shi, *J. Phys. Chem. C* 115 (2011) 13329–13337.
- [60] J.M. Mayer, *Acc. Chem. Res.* 44 (2011) 36–46.
- [61] H.-J. Zhai, X.-H. Zhang, W.-J. Chen, X. Huang, L.-S. Wang, *J. Am. Chem. Soc.* 133 (2011) 3085–3094.
- [62] E.C. Tyo, M. Nossler, R. Mitric, V. Bonacic-Koutecky, A.W. Castleman, *Phys. Chem. Chem. Phys.* 13 (2011) 4243–4249 (references therein).
- [63] K. Kwapien, M. Sierka, J. Döbler, J. Sauer, M. Haertelt, A. Fielicke, G. Meijer, *Angew. Chem. Int. Ed.* 50 (2011) 1716–1719.
- [64] X.-L. Ding, W. Xue, Y.-P. Ma, Z.-C. Wang, S.-G. He, *J. Chem. Phys.* 130 (2009) 014303.
- [65] X.-N. Wu, Y.-X. Zhao, S.-G. He, X.-L. Ding, *Chinese J. Chem. Phys.* 22 (2009) 635–641.
- [66] J.-B. Ma, X.-N. Wu, Y.-X. Zhao, X.-L. Ding, S.-G. He, *Chinese J. Chem. Phys.* 23 (2010) 133–137.
- [67] Y.-P. Ma, X.-L. Ding, Y.-X. Zhao, S.-G. He, *ChemPhysChem* 11 (2010) 1718–1725.
- [68] J.-B. Ma, X.-N. Wu, Y.-X. Zhao, S.-G. He, X.-L. Ding, *Acta Phys. Chim. Sin.* 26 (2010) 1761–1767.
- [69] X.-L. Ding, X.-N. Wu, Y.-X. Zhao, J.-B. Ma, S.-G. He, *ChemPhysChem* 12 (2011) 2110–2117.
- [70] With the Sc₂O₃ density of 3.84 g/cm³, the diameters of Sc₃₀O₄₅⁺ and Sc₄₄O₆₆⁺ (round balls) are calculated to be 1.20 and 1.36 nm, respectively.
- [71] M. Che, *A.J. Tench, Adv. Catal.* 31 (1982) 77–133.
- [72] A. Bruckner, *Chem. Soc. Rev.* 39 (2010) 4673–4684.
- [73] B. Xu, Y.-X. Zhao, X.-N. Li, X.-L. Ding, S.-G. He, *J. Phys. Chem. A* 115 (2011) 10245–10250.
- [74] J.-B. Ma, X.-N. Wu, Y.-X. Zhao, X.-L. Ding, S.-G. He, *J. Phys. Chem. A* 114 (2010) 10024–10027.
- [75] Z.-C. Wang, T. Weiske, R. Kretschmer, M. Schlangen, M. Kaupp, H. Schwarz, *J. Am. Chem. Soc.* 133 (2011) 16930–16937.



Sheng-Gui He was born in Anhui province of China on February 9, 1974. He received a B.S. degree in physics and a Ph.D. degree in chemistry from University of Science and Technology of China in 1997 and 2002, respectively. After postdoctoral stays at University of Kentucky (September 2002–February 2005) with Professor Dennis J. Clouthier for laser spectroscopy and at Colorado State University (February 2005–January 2007) with Professor Elliot R. Bernstein for photo ionization mass spectrometry, he joined Institute of Chemistry, Chinese Academy of Science in January 2007. His research interests are experimental and theoretical studies of reactive intermediates including free radicals and atomic clusters.